Atomistic Simulation of the Water Influence on the Local Structure of Polyamide 6,6

Sylvain Goudeau,*,† Magali Charlot,‡ Caroll Vergelati,‡ and Florian Müller-Plathe†

International University Bremen, Campus Ring 6, 28759 Bremen, Germany, and Rhodia Recherches, 85 rue des Frères Perret, 69192 Saint-Fons Cedex, France

Received January 22, 2004; Revised Manuscript Received August 2, 2004

ABSTRACT: To understand, at a molecular scale, the effect of water on the structure of the amorphous region of polyamide 6,6 (PA6,6), atomistic molecular dynamics simulations have been carried out. Our results concerning the very local water organization relative to PA moieties agree qualitatively with a two-step sorption model. The first sorption mode seems to be saturated well below the lowest water concentration studied (5% relative to the amorphous phase). Moreover, above this saturation, the overall water organization displays at 300 K larger clusters than the 2−3 molecules usually assumed in the literature. The temperature dependence of free volume, hole size, and hydrogen bonding has also been investigated. It shows a transition between plasticized and antiplasticized behavior.

Introduction

The variations of polyamide properties as a function of water content have been extensively studied "macroscopically". Dynamic mechanical analysis, calorimetric, and dielectric measurements have been the main tools involved in such studies.[1−3] They yielded several hypotheses about the role of water/amide hydrogen bonding in the resulting macroscopic properties. In particular, the decrease of the main relaxation temperature T_α (obtained from dynamical mechanical analysis, DMA) as a function of water content displays a critical behavior at a concentration c^* of one water molecule per three amide groups, for both polyamide (PA) 6 and 6,6. Above this threshold, a much slower decrease in T_α is observed. This has been interpreted[3] as most of the intermolecular amide−amide bonds available to water being broken below c^*. It is also inferred that most of the amide groups are actually not available to water, since c^* is much lower than 1. Local analysis methods, such as positron annihilation lifetime spectroscopy (PALS), provide a more detailed insight into the very local structural changes caused by water presence, although averaged over large samples.[4,5] The variation of the free volume hole size upon water sorption displays a minimum (for PA6) for a concentration c^* which is slightly lower than the one determined by DMA. Beyond c^*, adding more water yields a strong increase of mean hole volume.[5]

The two-step model proposed by Starkweather[6] is usually acknowledged to explain most of these features, namely the moisture-dependent mechanical relaxations in polyamide[1] and the density and free-volume variations. Qualitatively, this model states that the first water molecules sorbed by a polyamide sample form two hydrogen bonds between two pendent carbonyl groups from different chains. This sorption mode is then saturated for around 1 molecule per 2 amide groups, corresponding to 7 wt % water. Additional water molecules cluster between these molecules and the remaining free NH groups, leading to another saturation concentration of around 3 molecules per 2 amide groups. In the case of PA6,6 it would correspond to 21−22% water, which is significantly higher than the 15−17% water solubility in the amorphous phase at 300 K, but a significant part of the amide groups is supposed to be unavailable to water. Within the concept of the two-step model, water molecules of the first class are termed as tightly bound and the latter as loosely bound.

The simulations carried out here are aimed at providing a quantitative description of local water/amide interactions and organization, allowing us to investigate the interplay between the additional free-volume (plasticization) and hydrogen-bond interactions ("antiplasticization") resulting from water presence. Simulations have already focused on water/polymer hydrogen bonding in the cases of poly(ethylene oxide)[7,8] (PEO), poly(vinyl alcohol) (PVA),[9] and various polyimides.[10] Nylon/water systems have also been simulated, but for rather different purposes: the solubility (free energy of sorption) of water in PA-6 has been modeled atomistically.[11] The effect of water on the crystal modifications of PA6,6 was simulated by Vergelati et al.[12] Permeation of water through and surface adsorption of water on aromatic polyamides has been studied by Kotelyanskii et al.[13]

To our knowledge, the influence of water on the structure of the amorphous polyamide has not been studied yet.

Model and Simulations

Simulations were carried out for models reproducing the amorphous phase of polyamide 6,6, either dry or with 5 or 10 wt % water added.[14] It corresponds roughly to 1 water molecule per 3 amide groups in the first case and 2 molecules per 3 amides in the latter. We have also tested, to a more limited extent, one system containing 2 wt % water. The models are monodisperse, 20-monomer-long chains, containing 40 amide groups (see Table 1 and Figure 1), ethyl- and propyl-terminated. The corresponding molecular weight (M_n) is around 4500 g/mol, which is lower than the typical experimental range of 12 000−20 000 g/mol with a polydispersity around 2.[15,16] The main significance of this discrepancy is that real polyamide chains can form entanglements,

† International University Bremen.
‡ Rhodia Recherches.
* To whom correspondence should be addressed: Tel 0049 (0)-421 200 3560; e-mail s.goudeau@iu-bremen.de.

10.1021/ma049848o CCC: $27.50
Published on Web 09/15/2004

Table 1. Composition of the Simulation Cells[a]

system type	small systems	big systems
PA6,6$_{(dry)}$	$N_{PA} = 3$	$N_{PA} = 24$
	$M_n = 3 \times 4500$ g/mol	$M_n = 24 \times 4500$ g/mol
	$N_a/N_w = 120/0$	$N_a/N_w = 120/0$
PA6,6$_{(+ 5 wt \% water)}$	$N_{PA} = 3$	$N_{PA} = 24$
	$M_n = 3 \times 4500$ g/mol	$M_n = 24 \times 4500$ g/mol
	$N_a/N_w = 120/38$	$N_a/N_w = 960/304$
PA6,6$_{(+ 10 wt \% water)}$	$N_{PA} = 3$	$N_{PA} = 24$
	$M_n = 3 \times 4500$ g/mol	$M_n = 24 \times 4500$ g/mol
	$N_a/N_w = 120/76$	$N_a/N_w = 960/608$

[a] N_{PA}, N_a, and N_w are the number of PA molecules, amide groups, and water molecules, respectively. We tested also one 2% water containing system, with $N_a = 960$ and $N_w = 152$.

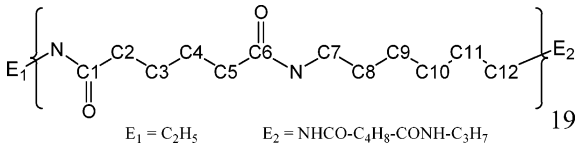

Figure 1. Structure of the polyamide chains employed in simulations.

which is not the case with chains of 4500 g/mol. However, considerations about entanglements are not really sensible at the atomistic scale, where a polymer segment hardly travels more than 1 nm throughout a simulation run, which is clearly not enough to feel the associated topological constraints. Therefore, we do not expect at such short time scales much bias from our choice of shorter chains. Two systems, containing 3 chains and 24 chains, have been investigated. The bigger systems were obtained by replicating the smaller ones twice in each direction. The size of the 20 000-atom (24 chains) systems is ca. 5−6 nm^3. Our simulation protocol consists of two procedures, namely chain generation (simulation of noninteracting chains) and subsequent classical molecular dynamics simulation of an atomistic model of bulk polyamide.

Chain Generation. A set of noninteracting chains has been generated by a pivot Monte Carlo method (PMC),[17] as implemented in the GMQ software developed by Brown.[18] In the PMC simulations, the Monte Carlo moves are random changes of randomly picked dihedral angles. This method has been proven to generate successfully meltlike conformations of the chains for a broad range of apolar and polar polymers, showing a good agreement with experimental mean radii of gyration (R_g) and end-to-end distances ($\langle r \rangle$).[19−23] It generates ensembles for a phantom chain, in which every atom interacts with neighboring atoms only if they are within a certain number of bonds along the chain. With this range correctly chosen, the ensemble corresponds to chains in a θ solvent or melt. A value of four backbone bonds has been chosen for PA, implying that two neighboring amide groups do not interact with each other.[24] By doing so, we avoid the formation of exclusively intramolecular hydrogen bonds between neighboring amides in the absence of compensating intermolecular ones. This leads to a slight overestimation of $\langle r \rangle$ (7.5 nm, averaged over 1000 configurations) compared to the experimentally available values of dimensions in θ solvents, estimated from ref 15 as 6.1 ± 0.6 nm for 4500 g/mol chains. Employing an interaction range of nine backbone bonds (so that neighboring amide groups fully interact) results in strongly underestimated $\langle r \rangle$, 3.7 nm. It is useless at this stage to optimize further the PMC parameters to get the best agreement with experimental $\langle r \rangle$ and R_g: because of the limited number of molecules, some simulation cells obtained with the four backbone bonds cut off have R_g and $\langle r \rangle$ as low as 1.5 and 3.5 nm, respectively. Eight starting configurations for further molecular dynamics simulations are evenly picked from a trajectory of 2×10^6 attempted PMC moves at 300 K, with an acceptance ratio of around 10%.

After this generation stage, the chains are submitted to periodic boundary conditions (PBC), with the full range of intra- and intermolecular nonbonded interactions taken into account, using classical atomistic molecular dynamics. Although this method has been shown to yield biased conformations at intermediate length scales in the case of model bead−spring chains[25] when a full interaction potential was quickly established among a set of initially noninteracting chains, we consider that it still allows to obtain realistic conformations and packing at the 1−2 nm length scale for polyamide. The upward shift of mean-square internal distances (for distances corresponding to 5−20 bonds) resulting in ref 25 from the push-off procedure is indeed expected in the case of polyamide due to intermolecular amide−amide interactions disregarded during the PMC stage, which tend to increase chain alignment at short length scales.

Molecular Dynamics. The preparation stage, necessary to introduce the intermolecular interactions representative of the polyamide melt, starting from a set of initially noninteracting chains, is composed of three steps:

(i) First, the box size is set arbitrarily to a rather high value, so that the density of the initial cell is around 0.85 g/cm^3 (the experimental value at room temperature is 1.07−1.1).

(ii) Then overlaps between initially noninteracting chains are removed at constant volume (around 10 MD stages of 2000 time steps each, during which the nonbonded ϵ parameters (see Table 2) are turned on progressively from 0 to their full value, and the time step is increased from 10^{-6} to 2 fs with a temperature coupling time equal to 10 time steps).

(iii) The final stage is carried out at constant pressure and temperature (NPT) for 2 ns at 500 K. The length of the time step is 2 fs. Temperature and isotropic pressure (1 atm) are regulated by Berendsen's method,[26] with coupling times of 0.2 and 5 ps (compressibility 10^{-6} kPa^{-1}), respectively. The chains do not have time to fold before the density reaches the equilibrated value of 0.99−1.03 g/cm^3, depending on water content. The introduction of water molecules, as described and justified in a further section, takes place at the beginning of this NPT stage at 500 K.

The cells are then submitted to a continuous cooling (0.25 K/ps) at constant pressure. The configurations extracted at the desired temperature from this cooling stage constitute starting points for further NPT simulations during which the properties of interest are analyzed. These production runs last 2 ns (big systems) or 6−10 ns (small ones). Configurations are extracted for analysis every 10 ps during the last 1 ns of the simulations. The length of the time step is 2 fs. The Berendsen thermostat and manostat are used with coupling times of 0.2 and 5 ps (isothermal compressibility 10^{-6} kPa^{-1}), respectively. A Verlet neighbor list with pair cutoff of 1.0 nm is used and updated by a link-cell scheme every 30 steps. Bond constraints are maintained to a relative tolerance of 10^{-6} by the SHAKE

Table 2. Force Field Parameters[a] for Polyamide 6,6

Bond constraints

Type	*Length (nm)*
$C_h - H$	0.109
$C_h - C_h$	0.1522
$C_h - C_a$	0.152
$C_h - N$	0.1449
$C_a - N$	0.1335
$N - H_n$	0.101
$C_a - O$	0.1229

Angle bending $V_{angles} = \frac{k_\phi}{2}(\phi - \phi_0)^2$

Type	Φ_0	K_Φ
$C_h - C_h - C_{h/a}$	111	250
$H - C_h - H$	109.5	145
$C_h - C_h - H$	109.5	150
$C_a - C_h - H$	109.5	210
$C_h - C_a - O$	120.4	335
$C_h - C_a - N$	116.6	293
$C_a - N - H_n$	120.0	125
$C_h - N - H_n$	120.0	209

Torsions $V_{tors} = \sum_p \frac{k_\tau}{2}[1 - \cos p(\tau - \tau_0)]$ (+ symbols below separate the different terms)

Type	*Periodicity p*	τ_0	k_τ
$C_h - C_h - C_h - C_h$	1 + 3	180	$2.0_{(1)} + 3.6_{(3)}$
$C_h - C_h - C_h - C_a$	1 + 3	180	$8.1_{(1)} + 3.6_{(3)}$
$C_h - N - C_a - C_h$	1 + 2	180	$25_{(1)} + 40_{(2)}$
$C_a - N - C_h - C_h$	1	180	9
$O - C_a - N - H_n$	1	180	35

Nonbonded interactions[b] $V_{nb} = \frac{q_i q_j}{4\pi\varepsilon_0}\left(\frac{1}{r_{ij}} + \frac{\varepsilon_{rf} - 1}{2\varepsilon_{rf} + 1}\frac{r_{ij}^2}{r_{cutoff}^3}\right) + 4\varepsilon_{ij}\left[\left(\frac{\sigma_{ij}}{r_{ij}}\right)^{12} - \left(\frac{\sigma_{ij}}{r_{ij}}\right)^6\right]$

Type	ε *(kJ/mol)*	σ *(nm)*	*q (e)*
H	0.0657	0.24 / 0.25	0.08229
H_n	0.0657	0.1	0.2819
C_h	0.458	0.35	-0.1506
C_a	0.360	0.35	0.5973
N	0.7118	0.33	-0.4057
O	0.8792	0.32	-0.5479

[a] C_h stands for a carbon involved in CH_2 or CH_3 groups, C_a for an amide carbon. In the same way, H is a CH_2 or CH_3 hydrogen and H_n an amide hydrogen. [b] Nonbonded interactions do apply fully between atoms interacting through torsion terms (1−4 interactions). The cutoff for these interactions is 0.9 nm; the reaction field dielectric constant ϵ_{rf} for electrostatic interactions is 5. The Lorentz−Berthelot combination rules are applied to determine the σ and ϵ parameters of unlike pairs: $\epsilon_{ij} = \epsilon_{ii}.\epsilon_{jj}^{0.5}$ and $\sigma_{ij} = (\sigma_{ii} + \sigma_{jj})/2$.

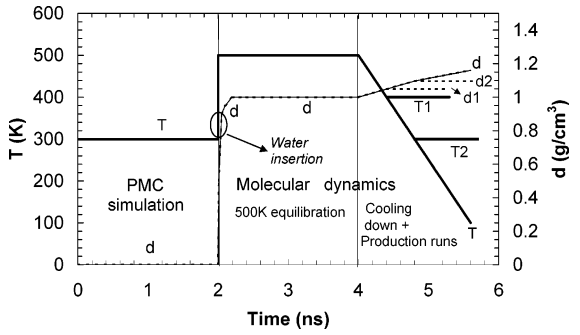

Figure 2. Density (dashed curve, d labels) and temperature (solid curve, T labels) during the various stages from chain generation to equilibration and production runs.

procedure.[27] The whole procedure from chain generation to production runs is represented in Figure 2.

The contents of the simulation cells and the parameters involving their time dynamics are displayed in Tables 1 and 2. The functional form of the force field employed and more details concerning the MD simulation program YASP can be found elsewhere.[28] The corresponding force field parameters for polyamide are given in Table 2. These parameters are partly derived from the all-atom model of *N*-methylacetamide (NMA) proposed by Caldwell et al.,[29] who had themselves modified the parameters of Jorgensen et al.[30] initially established for united-atom NMA in the framework of the more general OPLS force field. We have left the bond lengths and angles describing the amide moieties unchanged, whereas the torsional and Lennard-Jones parameters have been slightly modified to obtain the correct density, heat of vaporization, and diffusion coefficients for liquid NMA within our MD package. This mainly implied a slight reduction of van der Waals radii of most atoms. The new parameters have then been checked against liquid ϵ-caprolactam and ported to PA amide moieties with minor modifications. For example, the Lennard-Jones radius of hydrocarbon hydrogens had to be reduced from 0.29 to 0.26 nm for NMA and then to 0.25 nm for ϵ-caprolactam. With the adapted parameters, the simulation of 200 NMA molecules and 120 ϵ-caprolactam molecules during cooling from 500 to 300 K with a cooling rate of 0.5 K/ps, followed by an NPT stage at 300 K, reproduced densities to within 2% of the experimental values and heats of vaporization to within 5%. The density of the amorphous phase of PA6,6 is not known with a great precision; experimental values[15,16] at 300 K range from 1.07 to 1.1 g/cm^3. Therefore, we initially tested two different force fields with the van der Waals radius of hydrocarbon hydrogens being 0.24 and 0.25 nm, yielding densities of 1.104 and 1.073 g/cm^3, respectively, at 300 K. As the specific volume difference between those systems is almost exactly balanced by the excluded volume around the hydrocarbon moieties, both force fields result in similar values for glass transition temperatures, Young moduli, water diffusion coefficients, and water overall distribution. For the sake of simplicity, we will consider mainly the high-density systems ($\sigma = 0.24$ nm), unless explicitly stated.

The parameters for torsions along the chain backbone, specific to PA, were adjusted to reproduce the energies obtained from ab initio calculations (Hartree−Fock, 6-31G basis set). The Gaussian package[31] was used to compute the torsional barriers around the amide group ($C_5-C_6-N-C_7$, $C_4-C_5-C_6-N$, $O-C_6-N-H$) for NMA, *N*-ethylacetamide, *N*-butylacetamide, and *N*-hexylacetamide.

Water Inclusion. Water is described by the SPC/E model.[32] Like in previous simulations of water-swollen polymers,[9,10,33] simple combination rules were used to include SPC water in the force field description of hydrogen-bonded, hydrated systems.

The interactions between various water models and amide groups have been extensively studied in simulations of biological molecules[34−36] and compared with ab initio data. The GROMOS and OPLS-AA force fields succeeded in reproducing the free energy of hydration of several methyl-substituted amides and amines[34,35] in contact with SPC or TIP4P water, without the requirement of additional polarization terms in the initial force fields. All condensed-phase energetic properties are perfectly reproduced.

The water molecules are added at the beginning of the first NPT stage at 500 K, as stated before. Molecules are inserted in a totally random way, regarding their position and orientation. In the literature, the simulations of water-containing polymer systems are often carried out at constant temperature, and water is introduced at bulk density at the beginning of the simulation. This allows the formation of 2−3-member small clusters,[13] starting from random water positions,

Table 3. Simulated Properties of the Amorphous Phase of PA6,6, vs Experimental Properties of the Semicrystalline Material (Exp-SC) and the Amorphous Phase (Exp-Amorphous)[a]

property	simulation	exp-SC[15,16]	exp-amorphous[15,16]
$d_{300\ K}$(dry)[b] [g/cm^3]	1.104	1.14	1.07−1.1
$\alpha_{(rubber)}$[c] [K^{-1}]	5.4×10^{-4}		
$\alpha_{(glass)}$[c] [K^{-1}]	2.8×10^{-4}		
$E_{300\ K}$(dry)[d] [GPa]	2.8 (2.3−3.0)	3.3	1.7
$D_{w\ 300\ K,10\ wt\ \%}$[e] [cm^2/s]	$<0.5 \times 10^{-8}$	0.2×10^{-8}	0.2×10^{-8}
$D_{w\ 350\ K,10\ wt\ \%}$[e] [cm^2/s]	6×10^{-7}	2×10^{-7}	2×10^{-7}
$D_{w\ 500\ K,10\ wt\ \%}$[e] [cm^2/s]	2.5×10^{-5}	2.7×10^{-5}	2.7×10^{-5}

[a] The experimental crystallinity of PA6,6 is roughly 50%. σ_H is 0.24 nm unless explicitly stated. [b] Density at 300 K measured during 1 ns at room pressure and 300 K in simulations (big systems). [c] Thermal expansion coefficients measured as the slope of the volume vs temperature curves displayed in Figure 4. The glass coefficient is measured between 150 and 300 K; the rubber one between 500 and 350 K. Values for dry PA. [d] Young's modulus at 300 K, obtained from the slope of stress vs strain during simulated uniaxial tensile tests, at a rate of 0.125 GHz (i.e., 12.5% strain per ns) in the 0−2% strain range. [e] Water oxygen diffusion coefficients obtained during 5 ns simulations (small systems only) at the indicated temperature. The diffusion coefficient D is computed according to the following relation, where $\mathbf{r}$ is the position vector of a water oxygen, and the average is performed over all time origins (0): $D = {}^1/_6 \lim_{t\to\infty}(d/dt)\langle(\mathbf{r}(t) - \mathbf{r}(0))^2\rangle$.

but the formation of larger-scale patterns at high polymer concentrations is precluded by the low diffusion coefficients of water at room temperature. Introducing water at 500 K, in our case, enables every molecule to travel the whole box size (5 nm) during the first nanosecond of equilibration. Visual observation and cluster analysis of simulations at 500 K show no phase separation; the available literature data (experiments and semiempirical Flory−Huggins fits) for PA6,6 melts[37,38] at such temperatures suggest a solubility of at least 11% water. The PA−water χ interaction parameter is increasing with temperature above 500 K[38] so the solubility should be higher at lower temperature. While we exclude the possibility, in these conditions, to freeze during the cooling procedure a phase-separated structure formed at higher temperatures, we cannot pretend to equilibrate water patterns that have a dimension close to the greatest displacement achieved by the constituent molecules, that is, around 1−2 nm at 350 K and 0.5−0.6 nm at 300 K. In this regard, the results obtained concerning water hydrogen bonding between amide groups can be considered as representative at 300 K, but larger scale patterns (5−10-molecule clusters) discussed further in the paper have been formed at 350 K or above.

The accuracy of our model can be discussed from the values presented in Table 3, displaying a comparison between simulated and experimental properties, where available. The Young's moduli displayed in Table 3 have been computed by submitting the cells to uniaxial strain: A strain rate of 1.25×10^8 s^{-1} is imposed on the final configurations of selected NPT runs by rescaling all atomic coordinates by a factor 1.00025 every 2 ps in a given direction. The pressure in this direction is not coupled to the manostat. The moduli values, independent of water content at such low time scales, are scattered between 2.3 and 2.8 GPa at 300 K, depending on the configuration and the direction investigated. This is lower than experimental values for semicrystalline PA6,6, but mechanical modeling studies[15] conclude that the presence of crystallites leads to an enhancement between 50 and 100% of the modulus of the purely amorphous polymer. Our values of Young's modulus would then be overestimated by 40% at most, which can be considered as a good agreement if we take into account the simulated strain rate, 10 orders of magnitude higher than in experiments.

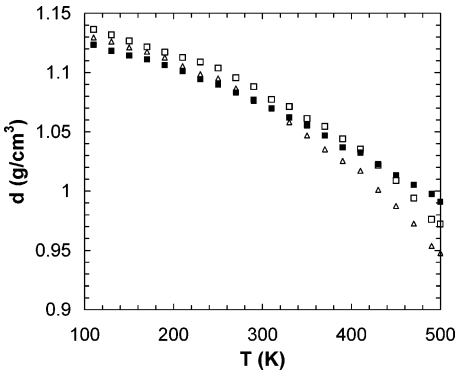

Figure 3. Density of PA6,6 cells as a function of temperature, averaged over six configurations for each water contents, simulated with (■) dry PA, (□) 5% water, and (△) 10% water with $\sigma_H = 0.24$ nm. Small systems: cooling rate 0.25 K/ps. The standard deviation is close to the symbol size.

True diffusive motion of water molecules is observed only above 400 K. As was noticed in previous studies[10,33] of other polymers, the mobility of water in the glassy polymer can be subdivided into two major components: hopping between different sites within the polymer and smaller length scale displacements corresponding either to isolated molecules moving inside cavities or to molecule exchange inside the same cluster of several molecules. The latter mode leads to subdiffusive behavior. Qualitatively, the main difference between water dynamics in PA and in the polymers simulated previously is the larger length scale (more than 1 nm) of subdiffusive processes which do not involve site−site hopping. As a result, the diffusive behavior in the mean-square displacement vs time curves at the nanosecond time scale is clearly observed only above 400 K. In the diffusive regime, the values of diffusion coefficients (D) at 500 K (2.5×10^{-5} cm^2/s) perfectly correspond to the value extrapolated from measurements between 300 and 375 K, assuming an Arrhenius temperature dependence of D with an activation energy of 58 kJ/mol.[16]

The simulated values obtained for density, glass temperature ($T_g = 330$ K), and expansion coefficients are all compatible with the experimental values, given the different time scales, and the uncertainties of experimental data initially obtained for semicrystalline materials (50% crystallinity), which have to be extrapolated to 0% crystallinity.

Results and Discussion

Volumetric Properties. Although we are interested here in a picture of water−PA structure and interactions around 300 K, it is necessary first to describe their development during the cooling stage from the initial temperature of 500 K. The data of this section have been obtained from the cooling runs from 500 to 100 K, at cooling rates of 0.25 K/ps, unless indicated otherwise.

The volumetric properties vs temperature (VT) curves are shown in Figures 3 and 4 not only for validation purposes but also as a first probe to test the overall water behavior in polyamide samples.

At room temperature, the experimental density displays an initial increase with water content up to a

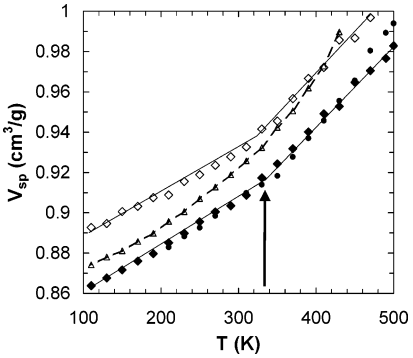

Figure 4. Specific volume of PA6,6 as a function of temperature (single configuration plots): (■) dry PA, (●) PA−2% water (same initial configuration), (◇) dry PA, $\sigma_h = 0.25$ nm, (△) PA−10% water, shifted by 0.02 cm^3/g upward for clarity. Arrow indicates the transition temperature. The cooling rate is always 0.25 K/ps.

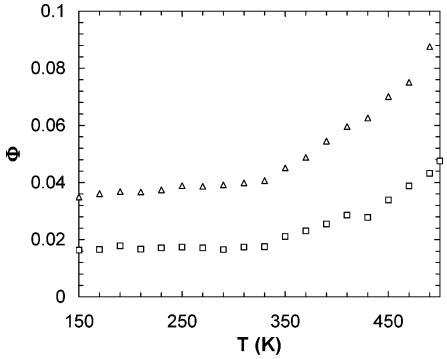

Figure 5. Additional volume fraction Φ due to (□) 5% water or (△) 10% water as a function of temperature. Big systems: cooling rate 0.25 K/ps.

concentration of around 10−12%, which is close to the saturation value (15−17%) measured in air of 100% relative humidity. Beyond this concentration of 10−12%, a strong drop in density is observed when more water is added. This is what is observed in Figure 3 but at lower temperatures (around 200 K). At 300 K, the density maximum in simulations is reached at lower water content, closer to 5% than 10% water. Further equilibration (2 ns) at 300 K leaves this feature unchanged. Such quantitative discrepancy (the qualitative trend is correct) is often found in simulations when a system is obtained by freezing at high cooling rates the conformations obtained at higher temperature.

A transition in the slope of the VT curves is observed (Figure 4) around 330 K for dry PA samples; this transition remains visible when small amounts of water, 2 wt %, are added. The water-containing samples (5% or 10%) show a continuous thermal expansion change from rubber to glasslike between 350 and 250 K. It has already been observed, including in simulations,[39] that a low-molecular-weight solvent increases the temperature width of the transition region. Therefore, the decrease in the volumetric transition temperature (T_g) provoked by water content cannot be measured in simulations. One would also expect to observe a higher T_g in simulation than in experiments due to the higher cooling rate. This usually leads to a 20−50 K excess. We find here T_g(sim) = 330 ± 10 K (dry PA) only 10 K or less above the experimental volumetric/calorimetric T_g,[15] which is however affected by the high crystallinity[40] of the samples.

Water and Free Volume. The effect of water on overall PA unoccupied volume can be evaluated by computing the difference of specific volume between dry PA and moist samples. The additional free volume fraction due to water is shown in Figure 5 and defined as

$$\Phi = \frac{V_{PA+H_2O} - V_{H_2O} - V_{dry}}{V_{dry}} \qquad (1)$$

where V_{PA+H_2O} is the volume per mole of cell of the water-containing polymer, V_{dry} that of the dry polymer, and V_{H_2O} that of the corresponding number of water molecules.

The excluded volume around water (V_{H_2O}) is assumed to be temperature independent and to correspond to hard spheres with radius 0.16 nm. Any value of V_{H_2O} in eq 1 is arbitrary; however, we have chosen here a volume (17 Å^3) significantly lower than the equivalent specific volume of a water molecule in bulk water (30 Å^3), obtained from the density of water at 300 K. Therefore, all water molecules are regarded as isolated. The absolute unoccupied volume fraction displayed in Figure 5 is then probably overestimated, particularly in the case of 10% water where a strong clustering is expected and effectively observed in simulations. It is, however, possible to extract the qualitative trends.

The additional free volume fraction Φ corresponds to the extra unoccupied volume caused by water sorption. It displays (Figure 5) a rather sharp transition around 340 K at both water contents, 5% and 10%. This temperature of 340 K is close to the volumetric T_g observed for the dry polymer. This is valid both for big and small systems and for both PA force fields (data not shown). These transitions in the free volume behavior are not related to water clustering (which occurs at higher temperature for 10% water than for 5%) but probably to the mobility of water molecules. At high temperatures, most molecules can be considered as unbound to PA; that is, their interactions with amide group are weak and short-lived and have little effect on their motion. This can be viewed as the "boiling" of water in PA cavities, resulting in an expansion of the unoccupied volume in the flexible polymer matrix. It can be noticed in Figures 3 and 5 that this effect is increased above 400−420 K. As the temperature is decreased, the fraction of unbound or loosely bound molecules decreases, and it is always greater for 10% water than for 5%. This will be quantified in the next section.

To investigate the validity of the concept of water hole filling at low temperature and water content, we have employed two methods to define and measure the cavities between the excluded volume areas in PA: The first method consists of fitting polyhedra into the cavities located between polymer chains. This method has the advantage to avoid the percolation of free volume observed at high temperature with probe sphere insertion methods. The initial position of the center of a "probe" polyhedron is chosen randomly. If the insertion position is such that the closest atom (PA or water) is more than 0.25 nm away, it is accepted. The position of this center is then moved toward the center of the cavity and optimized to give the largest hole volume. The volume itself is computed as a polyhedron (32 faces) taking into account the van der Waals radii of the neighboring atoms; each face of the polyhedron is moved away from the center until it enters into contact with the closest atom. The second method relies on the

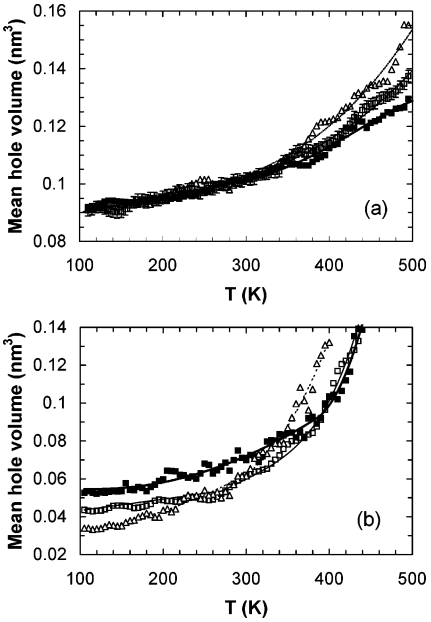

Figure 6. Average hole volume as a function of temperature, as obtained using a polyhedron method (a) or using the SURFNET[41] software (b): (■) dry polymer, (□) 5%, and (△) 10% water (big systems).

SURFNET program[41] which measures the probe accessible volume based on a grid defining occupied and vacant sites. The grid interval is set to 0.5 Å and the probe radius to 1.15 Å. Since periodic boundary conditions are not handled by the program, holes close to the boundaries are excluded. We also exclude cavities of too small volume (<0.03 nm^3) by averaging the volume of the 15 biggest holes only. Both methods use the same atomic van der Waals radii to define the intersection between the probe or polyhedron and an atom in the cell: $R_O = 0.14$ nm for an oxygen, $R_C = 0.19$ nm for a carbon, $R_N = 0.16$ nm for a nitrogen, hydrogen atoms are disregarded. Reducing R_C (to 0.15 nm) and including explicitly the hydrogens results in similar trends for hole volumes (as checked for a limited number of configurations) but at the price of considerably increased computing times. The volumes obtained by the first and second method are plotted respectively in parts a and b of Figure 6.

Both methods reveal that above 350 K the addition of 10% water leads to a net increase in average hole volume. This increase is lower for 5% water, with a more drawn-out onset temperature range, between 350 and 420 K. Below these temperatures, the hole size is roughly the same for dry and moist PA according to the polyhedron method, whereas the SURFNET method leads to a continuous reduction of free volume with water contents at very low temperatures and an intermediate behavior at room temperature where the hole size minimum is for 5% water. This qualitatively different trend at low temperature can be easily understood as a consequence of the resolution of both methods: the PA cavities are by themselves always bigger for water-containing systems. What makes the hole sizes identical in Figure 6a is their partial filling by water molecules. The probe-accessible volume is more affected by the presence of such molecule than the geometrical one, since the hole radius (0.2−0.3 nm) is not much greater than the probe one (0.115 nm).

These plots can be only qualitatively compared to the average hole size obtained experimentally by positron annihilation lifetime spectroscopy[4,5] (PALS) due to the complex interaction between positronium and matter around the cavity, whereas simulated hole volumes are instantaneous snapshots of the system geometry. With this proviso, the simulated variation of hole size vs temperature for PA6,6 happens to agree qualitatively with PALS results for PA6 in a limited temperature range: from 0.07 nm^3 at 300 K to 0.11 nm^3 at 400 K.[5] A slightly different packing can be expected for PA6,6, but previous measurements from the same authors[4] provided 0.08 nm^3 at 300 K both for PA6 and PA6,6. The variation of PALS hole sizes with water content at room temperature displays experimentally an initial decrease up to 3−4% water, followed by a dramatic increase upon further water addition. The initial decrease is totally compensated for water contents greater than 5 wt %. We do not expect the SURFNET method and PALS experiments to yield the same "hole" volumes in the full [100−500 K] temperature range. This is obvious at high temperatures, where the average hole volume obtained through the SURFNET method diverges due to the percolation of ellipsoid-shaped holes in the instantaneous configuration snapshots. However, at intermediate temperatures (350 K), we notice that the aforementioned PALS trend of free volume variation with water contents is also observed through the SURFNET method, with a slight upward temperature shift which may be attributed to dynamical effects. The initial decrease at low water content, referred to as "hole filling", is consistent with the first stage of the two-step model due to water bridges between neighboring amides or water molecules directly attached to amide groups. According to this model, additional molecules (second stage) would be more loosely bound and more mobile and lead to significant chain spacing, thus more free volume. This is checked in the next part, detailing the water distribution at room temperature.

A last remark concerning the temperature-dependent packing of PA deals with the "plasticization" temperatures of 350 K for 10% and 5% water: these temperatures are obtained from a comparison between water-containing and dry systems. Strictly speaking, the onset of plasticization begins after the first stage of hole filling (probably between 2 and 3% water), so we should have taken such a system as the reference, and not the dry one, to compute the plasticization temperature from the additional specific volume. We have done some tests with 2% water (only one configuration tested), and the corresponding hole size statistics are not significantly different from the dry polymer.

Structure at Room Temperature. Experimental findings concerning PA structure and dynamics as a function of temperature and water contents are often explained with a dual sorption model. Our simulations are analyzed in the framework of this concept in order to determine whether water molecules can be classified as tightly bound, loosely bound, or not bound at all to PA in a static picture at room temperature (300 K). Unless explicitly stated, the data presented in this section have been averaged over the last nanosecond of 2 ns simulations.

The water−amide hydrogen-bond interactions have been analyzed. They are considered as (i) amide NH as the donor and water oxygen as the acceptor and (ii) water OH as the donor and amide oxygen as the acceptor. Considering the amide nitrogen as an acceptor for water leads to very few additional bonds—between

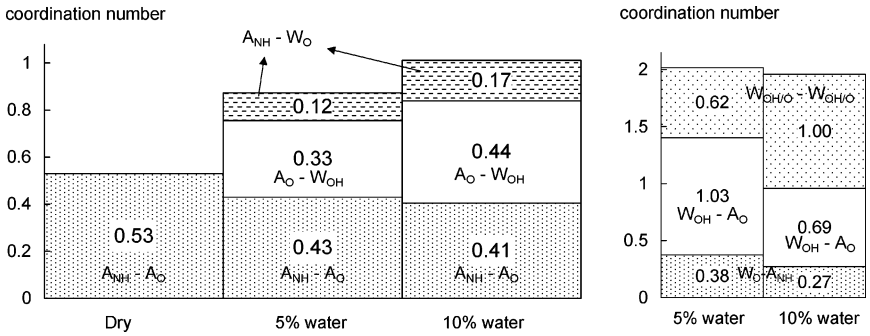

Figure 7. Hydrogen-bond coordination numbers relative to amide groups (a) and water (b). The acceptor and donor amide groups are labeled A_O and A_{NH}, respectively, the water OH donor groups W_{OH} and the water acceptor W_O.

2 and 5 per cell, less than 1%—so this type of interaction was neglected.

The hydrogen bonds are defined according to a simple geometric criterion: the distance between the hydrogen of the donor group and the acceptor has to be below 0.245 nm and the donor−hydrogen−acceptor angle above 130°. According to these definitions, the fraction of "unbound" water molecules that do not share hydrogen bonds with any amide group at a given time is only 20% for 5% water and rises to 40% for 10% water, while the ratio of the amide groups that are not bound to any water molecule decreases only slightly from 65% to 55% (values at 300 K). It means that around half of the amide functions are not available for water−PA hydrogen bonding, causing additional water molecules to accumulate into existing clusters. This is consistent with the critical concentration of 3−4% water obtained in PALS and dynamical analysis for the transitions in free volume behavior or T_α variations, instead of the 7%, 1 water for two amides, which should be observed if all amide groups were available. The fractions of amide groups and water molecules involved in amide−water or amide−amide or water−water bonds are represented in Figure 7. The average coordination number per amide group (number of amide−amide hydrogen bonds per amide group) is around 0.54 at 300 K for dry PA. The presence of 5% water at this temperature brings it to 0.43, which means that approximately 20% of PA−PA hydrogen bonds are broken. The 5% decrease in PA density resulting from water presence is then responsible only for a fraction of these broken bonds. It means that a significant number of water−amide H-bonds actually replaced amide−amide ones. The number of bridging water molecules, that is, hydrogen bonded to two different PA amide oxygens, is close to 1 per 10 amide groups. Roughly 1 molecule out of 3 is involved in a bridge.

If we consider now an amount of 10% water, we notice that only very few additional amide−amide hydrogen bonds are broken. The internal coordination number is 0.41. The fact that it remains unchanged with 5 or 10% water correlates quite well with DMA results,[3] which show only a slow decrease of T_α with water content above 5%. It is also surprising to notice that the qualitative variations of the coordination numbers obtained here are almost the same as those provided by Borodin et al.[7,8] in the totally different case of PEO, miscible with water, or Müller-Plathe[33] in the case of poly(vinyl alcohol). The number of water molecules bridging two different amide groups is still at 1 per 10 amide groups. Thus, only one water molecule out of six forms such a bridge.

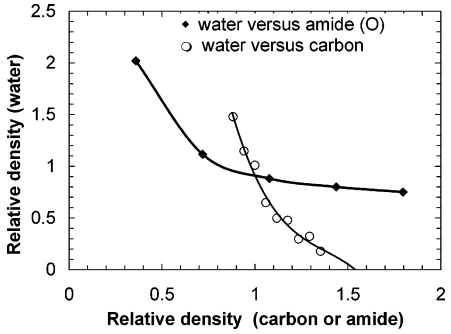

Figure 8. Water environment of an amide group as a function of the local density of neighboring amide groups or carbon atoms. These densities are defined within a sphere of 0.5 nm radius around the C−N center of mass of the central amide. The density of 1 for water corresponds to 0.94 molecules within the sphere. The carbon and amide density themselves are not strongly correlated within these 0.5 nm spheres (correlation coefficient ~0.04).

To establish which of these amide groups are not available to water, the water environment of an amide, averaged over all amide groups in the system, has been plotted in Figure 8 for 10% water as a function of the local surrounding amide and carbon density. For each amide group, we count the number of water molecules, neighboring amide groups, and methylene carbons within a sphere of radius 0.5 nm. The numbers of water molecules are grouped into bins corresponding to given numbers of amide or methylene carbon groups, then averaged, and rescaled to obtain the data of Figure 8.

At low PA carbon or amide density, or high water contents, both water vs carbon and water vs amide density curves are roughly hyperbolas (the very low carbon or amide density part of these curves has not been displayed). This is expected, as water simply takes up a volume corresponding to the volume vacated by the polymer. At higher PA densities (greater than 1) the situation is different and not determined by simple excluded-volume effects.

The presence of high carbon density regions prevents water from accessing amide groups. At a relative density of 1.2 for carbon, corresponding roughly to the density of the crystalline moieties, the number of water close neighbors of an amide is less than one-third of the average. Thus, the amide groups in such regions surrounded by alkane moieties can be considered as largely unavailable to water.

The water vs amide density curve does not decrease very much for amide relative densities between 1 and 1.5. This kind of "saturation" is due to the hydrophilicity of the amide groups, but we would even have expected

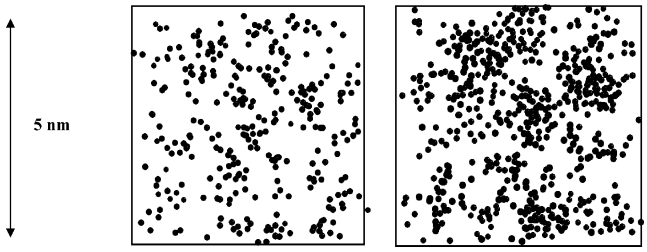

Figure 9. Snapshot of a simulation cell at 300 K: (a) 5% water, (b) 10% water. Each particle represents a water molecule. On the 2D representation of the system containing 10% water, what appears as water agglomerates is actually the projection of several smaller clusters lying on different backgrounds.

at least a slight increase of water density in these conditions, since carbon and amide density are not correlated in these amide-centered spheres. Indeed, the relative amide density between 1 and 1.5 corresponds respectively to 2 and 3 amides within the sphere at constant carbon density. And yet we do not observe, on average, additional water molecules in the sphere which would be bound to this third amide group. Therefore, irrespective of carbon density, the presence of already established amide−amide interactions results in lower water concentration; the amide−amide bonds in very high amide density regions are not easily broken or attractive to water.

45% of the amide functions have no water neighbor within 0.5 nm because they are situated in regions of higher density and rich in amide/amide intermolecular contacts. Only 3% of the amides have more than three water neighbors within this distance (0.5 nm), which confirms the experimental hypothesis that no more than three water molecule can fit into the vicinity of an amide group.

The resulting overall water distribution, following the local density patterns, is highlighted on the simulation snapshots of water containing systems at 300 K (Figure 9). Although no more than three water molecules share the immediate vicinity of an amide group, some much bigger clusters can be noticed in Figure 9. As stated before, the local density patterns resulting in the presence of such clusters have been formed at higher temperatures (above the volumetric T_g between 320 and 340 K) and are mainly frozen-in at room temperature. A simple cluster analysis shows "percolation" of such clusters for 10% water: it is always possible to find a path linking all molecules in the system, if the critical oxygen−oxygen distance below which two molecule are considered as cluster neighbors is chosen above 0.28 nm. Physically sensible values are between 0.3 and 0.35 nm. However, this does not reveal a cocontinuous, phase-separated system but rather smaller clusters (15−20 molecules at most) bridged by strings of 2 or 3 molecules. A more quantitative analysis of the actual clustering behavior is obtained by restraining the clusters to have a spherical shape and a water density above a critical value ρ_{min}. It is carried out in the following way: for each water molecule, we set up a list of neighboring molecules, sorted in order of increasing oxygen−oxygen distance. If any neighbor of that molecule is found within 3.3 Å, it is considered as connected and belonging to the same cluster, as in standard cluster analysis. When more than three molecules belong to the same cluster, a further requirement to consider additional molecules in the cluster is that the mass density

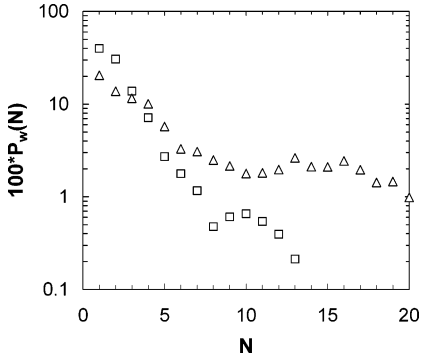

Figure 10. Distribution function of water molecules according to the size of the clusters they belong to. $P_w(N)$ is the probability of finding a water molecule in a cluster of N molecules: (□) 5% water, (△) 10% water.

Table 4. Percentage of Molecule Involved in Different Cluster Categories

% of molecules involved in	5% H_2O cutoff 0.31 nm	5% H_2O cutoff 0.33 nm	10% H_2O cutoff 0.33 nm
isolated molecules	26	24	8
2−4 molecule clusters	30	26	5
5−10 molecule clusters	44	50	87
>10 molecule clusters	12[a]	13[a]	16[a]

[a] Values in the last row (>10 molecule clusters) refer to clusters of spherical shape and minimal water density of 0.9 g/cm^3. Other numbers refer to usual cluster analysis. The cutoff defines the maximum distance below which two molecules are regarded as bonded.

ρ must remain above a critical value. The density is measured in a sphere centered at the center of mass of the growing cluster, and the radius of the sphere is delimited by the oxygen position of the candidate molecule. Figure 10 displays the distribution function of the water molecules according to the size of the cluster they belong to, for $\rho_{min} = 0.9$ g/cm^3. The bimodal aspect of the distribution of water molecules according to their cluster size is due to poor statistics beyond 8−9 molecule clusters. These bigger clusters represent only a small part of the total number of water molecules and appear only a dozen times during the nanosecond of analysis, as shown in Table 4. While most of the 2−3 molecule clusters have a detectable lifetime at 300 K (10% of them subsist throughout the simulation; the average lifetime of the others is around 250 ps), this lifetime increases dramatically with cluster size so that all clusters of more than seven molecules remain present during the 2 ns of production run.

To check whether free volume at chain ends can be accessed by water, implying a preferred location of bigger clusters around terminal monomers, we have plotted in Figure 11 the pair distribution functions of selected water/methylene carbon (C3) or (C9) pairs, as a function of the position of these carbons along the backbone.

The pronounced peak at 0.35 nm in the end-carbons−water oxygen radial distribution function displayed by 5% and 10% water systems reveals that the additional free volume around chain ends is effectively accessed and occupied by water. The water concentration is obviously depleted in the close and intermediate vicinity of the 4- and 6-membered carbon chains, except around 0.5 nm, which corresponds to the closest amide of C3. Because the water preference for chain ends depends on their chemical nature, it is difficult to speculate

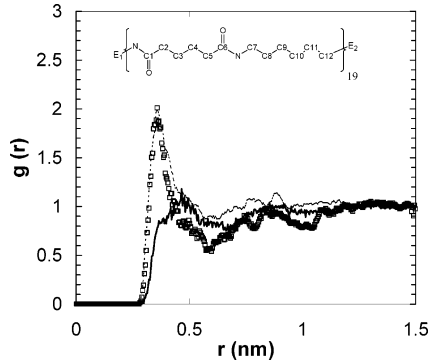

Figure 11. Radial distribution function (RDF) of (C3/water oxygen) or (C9/water oxygen) pairs; see inset for carbon labeling. The bold solid curve corresponds to the average over all pairs (5% water). Open squares: 10% water, the two terminal carbons only are accounted for. Thin dotted line: ditto, 5% water. The RDF for all pairs and 10% water has been omitted for clarity, being very similar to the RDF obtained with 5% water.

whether we overestimate or underestimate this effect in our simulations with alkane-terminated chains. The hydrophilic nature of the amine and carboxyl end groups present in real polyamide 6,6 should increase water preference for chain ends, but such end groups also tend to form hydrogen bonds with neighboring chains, resulting in lower free volume. Their concentration in the amorphous phase of PA is also a critical parameter. Reproducing both the experimental molecular weight and polydispersity of real PA chains is, however, beyond the scope of fully atomistic simulations.

Conclusions

The static water structure and distribution in polyamide samples have been investigated through atomistic simulations as well as its temperature dependence, which highlights some transitions between plasticized and antiplasticized behavior. Plasticization (in the sense of a net increase of excess free volume for water-loaded systems) occurs above 340 K, close to the simulated transition of the thermal expansion coefficients (320 K) of dry samples. Below this temperature, there is an interplay between the two behaviors hole-filling and plasticization. These features are compatible with the current descriptions (two-step sorption model) used to explain structural and mechanical properties of water-loaded PA as a function of frequency and temperature. The structure of hydrogen-bonding and water-clustering at room temperature is also consistent with the dual sorption model. However, the simulations extend beyond the "saturation" of this model and describe the water behavior also at higher concentrations. Features in the water structure occur already at relatively low concentration because of strong local density heterogeneities and lead to bigger clusters—located in particular at chain ends—than the three-molecule clusters foreseen by the two-step model. Moreover, it was shown here that half of the amide groups are not accessed by water molecules. Analysis of their environment shows that they are buried in regions of high alkane moieties density. These regions have a dimension of ca. 1−2 nm, correlated to the size of local density fluctuations in the amorphous samples.

Acknowledgment. This work was funded by the BMBF (German Federal Ministry for Education and Research), Grant 03N6015. The Fonds der Chemischen Industrie is also gratefully acknowledged. S.G. thanks David Brown for supplying the GMQ molecular dynamics code. The NIC (John von Neumann Institute for Computing) has significantly contributed to this work by providing computing time on the JUMP machine at the ZAM Center, Jülich, Germany.

References and Notes

(1) Laredo, E.; Hernandez, M. C. *J. Polym. Sci., Part B* **1997**, *35*, 2879−2888.
(2) Pathmanathan, K.; Cavaillé, J. Y.; Johari, G. P. *J. Polym. Sci., Part B* **1992**, *30*, 341−348.
(3) Le Huy, H. M.; Rault, J. *Polymer* **1994**, *35*, 136−139.
(4) Dlubek, G.; Stolp, M.; Nagel, C.; Fretwell, H. M.; Alam, M. A.; Radusch, H. J. *J. Phys.: Condens. Matter* **1998**, *10*, 10443−10450.
(5) Dlubek, G.; Redmann, F.; Krause-Rehberg, R. *J. Appl. Polym. Sci.* **2002**, *84*, 244−255.
(6) Starkweather, H. W. In *Water in Polymers*; ACS Symposium Series 127; American Chemical Society: Washington, DC, 1980; p 433.
(7) Borodin, O.; Bedrov, D.; Smith, G. D. *J. Phys. Chem. B* **2002**, *106*, 5194−5199.
(8) Smith, G. D.; Bedrov, D.; Borodin, O. *Phys. Rev. Lett.* **2000**, *85*, 5583−5586.
(9) Müller-Plathe, F.; van Gunsteren, W. F. *Polymer* **1997**, *38*, 2259−2268.
(10) Brown, D.; Neyertz, S.; Douanne, A.; Bas, C.; Alberola, N. D. *J. Phys. Chem. B* **2002**, 106, 4617−4631.
(11) Knopp, B.; Suter, U. W.; Gusev, A. A. *Macromolecules* **1997**, *30*, 6107−6113.
(12) Vergelati, C.; Imberty, A.; Perez, S. *Macromolecules* **1993**, *26*, 6, 4420−4425.
(13) Kotelyanskii, M. J.; Wagner, N. J.; Paulaitis, M. E. *Comput. Theor. Polym. Sci.* **1999**, *9*, 301−306.
(14) These percentages are related to the weight of dry PA; the overall water contents of the resulting cells are exactly 4.8 and 9.1 wt %, respectively.
(15) Viers, B. D. Nylon 6,6. In *Polymer Data Handbook*; Mark, J. E., Ed.; Oxford University Press: New York, 1999; p 190.
(16) Mehta, R. H. Physical constants of various polyamides. In *Polymer Handbook*, 4th ed.; Brandrup, J., Immergut E. H., Eds.; Wiley: New York, 1999; p V121.
(17) Neyertz, S.; Brown, D. *J. Chem. Phys.* **2001**, *115*, 708−717.
(18) Brown, D. *The gmq User Manual*, Version 3: http://www.univ-savoie.fr/labos/lmops/brown/gmq.html, 1999.
(19) Brown, D.; Clarke, J. H. R.; Okuda, M.; Yamazaki, T. *J. Chem. Phys.* **1994**, *100*, 1684−1692.
(20) Brown, D.; Clarke, J. H. R.; Okuda, M.; Yamazaki, T. *J. Chem. Phys.* **1994**, *100*, 6011−6018.
(21) Brown, D.; Clarke, J. H. R.; Okuda, M.; Yamazaki, T. *J. Chem. Phys.* **1996**, *104*, 2078−2082.
(22) Neyertz, S.; Brown, D.; Clarke, J. H. R. *J. Chem. Phys.* **1996**, *105*, 2076−2088.
(23) Neyertz, S.; Brown, D. *J. Chem. Phys.* **1995**, *102*, 9725−9735.
(24) For technical reasons, the PMC simulations of polyamide 6,6 with the GMQ package required force field parameters slightly different from those presented in Table 2. A simplified model was used, with a charge 0 on all atoms belonging to methylene moieties, −0.5e and +0.5e on the carbonyl oxygen and carbon, respectively, and −0.3e and +0.3e on the amide nitrogen and hydrogen, respectively. This provides electroneutrality in the treatment of the short-range nonbonded interactions.
(25) Auhl, R.; Everaers, R.; Grest, G. S.; Kremer, K.; Plimpton, S. J. *J. Chem. Phys.* **2003**, *119*, 12718−12728.
(26) Berendsen, H. J. C.; Postma, J. P. M.; van Gunsteren, W. F.; DiNola, A.; Haak, J. R. *J. Chem. Phys.* **1984**, *81*, 3684−3690.
(27) Müller-Plathe, F.; Brown, D. *Comput. Phys. Commun.* **1991**, *64*, 7−14.
(28) Müller-Plathe, F. *Comput. Phys. Commun.* **1993**, *78*, 77−94.
(29) Caldwell, J. W.; Kollman, P. A. *J. Phys. Chem.* **1995**, *99*, 6208−6219.
(30) Jorgensen, W. L.; Swenson, C. J. *J. Am. Chem. Soc.* **1985**, *107*, 569−578.
(31) Frisch, M. J.; Trucks, G. W.; Schlegel, H. B.; Scuseria, G. E.; Robb, M. A.; Cheeseman, J. R.; Zakrzewski, V. G.; Montgomery, J. A., Jr.; Stratmann, R. E.; Burant, J. C.; Dapprich, S.; Millam, J. M.; Daniels, A. D.; Kudin, K. N.; Strain, M. C.; Farkas, O.; Tomasi, J.; Barone, V.; Cossi, M.; Cammi, R.; Mennucci, B.; Pomelli, C.; Adamo, C.; Clifford,

S.; Ochterski, J.; Petersson, G. A.; Ayala, P. Y.; Cui, Q.; Morokuma, K.; Malick, D. K.; Rabuck, A. D.; Raghavachari, K.; Foresman, J. B.; Cioslowski, J.; Ortiz, J. V.; Stefanov, B. B.; Liu, G.; Liashenko, A.; Piskorz, P.; Komaromi, I.; Gomperts, R.; Martin, R. L.; Fox, D. J.; Keith, T.; Al-Laham, M. A.; Peng, C. Y.; Nanayakkara, A.; Gonzalez, C.; Challacombe, M.; Gill, P. M. W.; Johnson, B.; Chen, W.; Wong, M. W.; Andres, J. L.; Gonzalez, C.; Head-Gordon, M.; Replogle, E. S.; Pople, J. A. *Gaussian 98*; Gaussian, Inc.: Pittsburgh, PA, 1998.

(32) Berendsen, H. J. C.; Grigera, J. R.; Straatsma, T. P. *J. Phys. Chem.* **1987**, *91*, 6269−6275.

(33) Müller-Plathe, F. *J. Chem. Phys.* **1998**, *108*, 8252−8263.

(34) Rizzo, C. R.; Jorgensen, W. L. *J. Am. Chem. Soc.* **1999**, *121*, 4827−4836.

(35) Rizzo, C. R.; Jorgensen, W. L. *J. Am. Chem. Soc.* **2000**, *122*, 2878−2888.

(36) Kaminski, G. A.; Stern, H. A.; Berne, B. J.; Friesner, R. A. *J. Phys. Chem. A* **2004**, *108*, 621−627.

(37) Schaffer, M. A.; McAuley, K. B.; Cunningham, M. F. *Polym. Eng. Sci.* **2003**, *43*, 639−646.

(38) Rackaitis, M.; Strawhecker, K.; Manias, E. *J. Polym. Sci., Part B* **2002**, *40*, 2339−2342.

(39) van der Vegt, N.; Briels, W. J.; Wessling, M.; Strathmann, H. *J. Chem. Phys.* **1999**, *110*, 11061−11069.

(40) Rotter, G.; Ishida, H. *J. Polym. Sci., Part B: Polym. Phys.* **1992**, *30*, 489.

(41) Laskowski, R. A. *J. Mol. Graph.* **1995**, *13*, 323−330.

MA049848O